Abstracts

The 26th Hiroshima International Symposium on Synchrotron Radiation

Materials Science using VUV-SX Synchrotron Radiation

March 10- 11, 2022

Faculty Club, Hiroshima University and Online

Hiroshima Synchrotron Radiation Center, Hiroshima University

Supported by

Higashihiroshima City

The Japanese Society for Synchrotron Radiation Research

Program

Oral Session

DAY 1 ・Thursday, 10 March, 2022

Opening (Chairperson: T. Okuda)

09:30 – 09:40 Greeting
Manabu ABE (*Vice President, Hiroshima University, Japan*)

09:40 – 10:10 Overview of HiSOR Activities
Kenya SHIMADA (*Director, Synchrotron Radiation Center, Hiroshima University, Japan*)

10:10 – 10:20 Break

Oral Session 1 (Chairperson: S. Ideta)

10:20 – 10:55 **Ilya BELOPOLSKI** (*RIKEN, Japan*)
"Observation of linked loops in a quantum ferromagnet: a new paradigm for topology in physics"

10:55 – 11:30 **Chaoyu CHEN** (*Southern University of Science and Technology, China*)
"Electronic Structure Study on the Intrinsic Magnetic Topological Insulator Mn-Bi-Te family"

11:30 – 12:05 **Jayita NAYAK** (*Indian Institute of Technology Kanpur, India*)
"Experimental evidence of six-fold degenerate Fermions in $PdSb_2$"

12:05 – 13:15 Lunch

Poster Session (Chairperson: H. Sato)

13:15 – 14:00	Student Short Oral Session (1~2 min/each)
14:00 – 16:00	Poster Session

Oral Session 2 (Chairperson: M. Sawada)

16:10 – 16:45	**Goro SHIBATA** (*Tokyo University of Science, Japan*) "Angle-dependent XMCD as a Probe of Anisotropic Spin-density Distribution"
16:45 – 17:20	**Yuichi YAMASAKI** (*National Institute for Materials Science, Japan*) "X-ray Magnetic Circular Dichroism in a Chiral Antiferromagnet"

DAY 2 ・Friday, 11 March, 2022

Oral Session 3 (Chairperson: H. Sato)

09:30 – 10:05	**Kazuki SUMIDA** (*Japan Atomic Energy Agency, Japan*) "Spin-Resolved Photoemission of Heusler-Type Weyl Ferromagnet Films"
10:05 – 10:40	**Yoshihiko TOGAWA** (*Osaka Prefecture University, Japan*) "Chirality-Induced Spin Polarization in Chiral Crystals"
10:40 – 11:00	Break

Oral Session 4 (Chairperson: H. Namatame)

11:00 – 11:35	**Yoshifumi TAKASHIMA** (*Nagoya University, Japan*) "Construction and Operation of Superconducting Bending Magnets in Aichi-SR"
11:35 – 12:10	**Masahiro KATOH** (*Hiroshima University, Japan*) "Recent Results from Design Study on HiSOR-2"
12:10 – 13:30	Lunch

Oral Session 5 (Chairperson: K. Matsuo)	
13:30 – 14:05	**Toru ASAHI** （*Waseda University, Japan*） ″Applications of the Generalized High Accuracy Universal Polarimeter (G-HAUP) to Solid State Sciences″
14:05 – 14:40	**Akinari YOKOYA** （*National Institutes for Quantum Science and Technology, Japan*） ″Exploring active structures of DNA repair protein XRCC4 using CD and SAXS″

Closing Session (Chairperson: T. Okuda)	
14:40 – 14:55	Student Award Ceremony
14:55 – 15:00	Closing Remarks

Oral Session

-Oral Session-

O01 Observation of Linked Loops in a Quantum Ferromagnet

Ilya Belopolski [a,b]

a RIKEN Center for Emergent Matter Science (CEMS), Japan
b Laboratory for Topological Quantum Matter and Spectroscopy (B7), Department of Physics, Princeton University, USA

O02 Electronic Structure Study on the Intrinsic Magnetic Topological Insulator Mn-Bi-Te family

Chaoyu Chen

Southern University of Science and Technology, China

O03 Experimental Evidence of Six-Fold Degenerate Fermions in $PdSb_2$

Jayita Nayak et al.

Max Planck Institute for Chemical Physics of Solids, Germany

O04 Angle-dependent XMCD as a Probe of Anisotropic Spin-density Distribution

Goro Shibata

Department of Applied Physics, Tokyo University of Science, Japan

O05 X-ray Magnetic Circular Dichroism in a Chiral Antiferromagnet

Yuichi Yamasaki

National Institute for Materials Science, Japan

O06 Spin-Resolved Photoemission of Heusler-Type Weyl Ferromagnet Films

Kazuki Sumida

Materials Sciences Research Center, Japan Atomic Energy Agency, Japan

O07 Chirality-Induced Spin Polarization in Chiral Crystals

Yoshihiko Togawa

Department of Physics and Electronics, Osaka Prefecture University, Japan

O08 Construction and Operation of Superconducting Bending Magnets in Aichi-SR

Yoshifumi Takashima[a,b]

a Synchrotron Radiation Research Center, Nagoya University, Japan
b Aichi Synchrotron Radiation Center, Japan

O09 Recent Results from Design Study on HiSOR-2

Masahiro Katoh[a,b]

a Hiroshima Synchrotron Radiation Center, Hiroshima University, Japan
b Institute for Molecular Science, National Institutes of Natural Sciences, Japan

O10 Applications of the Generalized-High Accuracy Universal Polarimeter (G-HAUP) to Solid State Sciences

Toru Asahi[a,b] and Kenta Nakagawa[c]

a Faculty of Science and Engineering, Waseda University, Japan
b Research Organization for Nano & Life Innovation, Waseda University, Japan
c Kanagawa Institute of Industrial Science and Technology (KISTEC), Japan

O11 Exploring active structures of DNA repair protein XRCC4 using CD and SAXS

Akinari Yokoya[a,b], Kai Nishikubo[b,a], Maho Hasegaw[b,a]

a National Institutes for Quantum Science and Technology, Institute for Quantum Life Science, Japan
b Graduate School of Science and Engineering, Ibaraki University, Japan

Observation of Linked Loops in a Quantum Ferromagnet

Ilya Belopolski [a,b]

[a] RIKEN Center for Emergent Matter Science (CEMS), Wako, Saitama 351-0198, Japan
[b] Laboratory for Topological Quantum Matter and Spectroscopy (B7), Department of Physics, Princeton University, Princeton, New Jersey 08544, USA

Keywords: Linking number, Weyl loop, topological quantum matter, mathematical knot theory, angle-resolved photoemission spectroscopy (ARPES), Seifert bulk-boundary correspondence

Quantum phases can be classified by topological invariants, which take on discrete values capturing global information about the quantum state. Over the past decades, these invariants have come to play a central role in describing matter, providing the foundation for understanding superfluids, magnets, the quantum Hall effect, topological insulators and Weyl semimetals. In this talk, I will introduce a remarkable linking number (knot theory) invariant associated with loops of electronic band crossings in the mirror-symmetric ferromagnet Co_2MnGa [1-4]. We disentangle this system's rich topological structure through bulk-sensitive soft X-ray and surface-sensitive vacuum ultraviolet angle-resolved photoemission spectroscopy. We directly observe three intertwined degeneracy loops in the bulk Brillouin zone three-torus, T^3, such that each loop links each other loop twice. Through systematic spectroscopic investigation of this linked loop quantum state, we explicitly draw its link diagram and conclude, in analogy with knot theory, that it exhibits linking number (2,2,2), providing a direct experimental determination of the topological invariant. On the sample surface, we further predict and observe Seifert boundary states protected by the bulk linked loops, suggestive of a Seifert bulk-boundary correspondence. Our observation of a quantum loop link motivates the application of knot theory to the exploration of quantum matter.

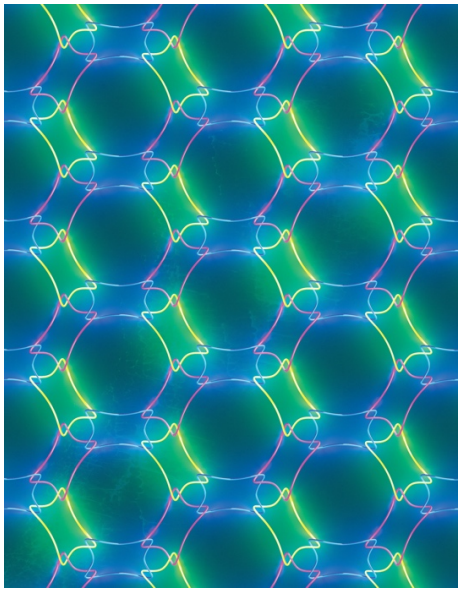

FIGURE 1. Mathematical link diagram in three-dimensional momentum space, characterizing the linking number of the linked Weyl loops (nodal lines) in the quantum ferromagnet Co_2MnGa, as characterized by ARPES.

REFERENCES

1. I. Belopolski *et al.* Observation of a linked loop quantum state. arXiv:2112.14722 and *Nature*, in press (2022).
2. I. Belopolski *et al*. Signatures of magnetic Weyl fermion annihilation in a correlated kagome magnet. *Phys. Rev. Lett.* 127, 256403 (2021).
3. I. Belopolski *et al.* Discovery of topological Weyl fermion lines and drumhead surface states in a room temperature magnet. *Science* 365, 6459 (2019).
4. M. Z. Hasan, G. Chang, I. Belopolski *et al.* Weyl, Dirac and high-fold chiral fermions in topological quantum matter. *Nat. Rev. Mat.* 6, 784 (2021).

19AG014, 19AG004, 19AU002, 19AU007, 19BG006, 19BG044, 19BU002, 19BU005 and 19BU012 BL-1 and Laser-ARPES

Electronic Structure Study on the Intrinsic Magnetic Topological Insulator Mn-Bi-Te family

Chaoyu Chen[a]

[a]*Southern University of Science and Technology*
Shenzhen 518055, China

Keywords: ARPES, Intrinsic magnetic topological insulator, topological surface state, gap.

The layered $MnBi_{2n}Te_{3n+1}$ family represents the first intrinsic magnetic topological insulator ever discovered, providing an ideal platform to explore novel areas of physics such as the quantum anomalous Hall effect at elevated temperature and axion electrodynamics. In this talk I will present our recent studies on the electronic structure, especially the topological surface state Dirac cone of $MnBi_{2n}Te_{3n+1}$ family, including:

1. Discovery of gapless surface states in antiferromagnetic topological insulator $MnBi_2Te_4$ [1]
2. The origin of gapless surface state in Mn-Bi-Te family: surface-bulk band hybridization [2]
3. Discovery of "half-magnetic topological insulator" with magnetic gap opening of surface state [3]
4. Realization of tunable surface gap in doped $MnBi_2Te_4$ [4]

These works have established a solid electronic platform for realizing quantum anomalous hall effect at elevated temperature.

REFERENCES

1. Yu-Jie Hao, Pengfei Liu, Yue Feng, Xiao-Ming Ma, Eike F. Schwier, Masashi Arita, Shiv Kumar, Chaowei Hu, Rui'e Lu, Meng Zeng, Yuan Wang, Zhanyang Hao, Hong-Yi Sun, Ke Zhang, Jiawei Mei, Ni Ni, Liusuo Wu, Kenya Shimada, Chaoyu Chen, Qihang Liu & Chang Liu. Gapless Surface Dirac Cone in Antiferromagnetic Topological Insulator MnBi2Te4. Physical Review X 9, 041038, doi:10.1103/PhysRevX.9.041038 (2019).
2. Xiao-Ming Ma, Zhongjia Chen, Eike F. Schwier, Yang Zhang, Yu-Jie Hao, Shiv Kumar, Ruie Lu, Jifeng Shao, Yuanjun Jin, Meng Zeng, Xiang-Rui Liu, Zhanyang Hao, Ke Zhang, Wumiti Mansuer, Chunyao Song, Yuan Wang, Boyan Zhao, Cai Liu, Ke Deng, Jiawei Mei, Kenya Shimada, Yue Zhao, Xingjiang Zhou, Bing Shen, Wen Huang, Chang Liu, Hu Xu & Chaoyu Chen. Hybridization-induced gapped and gapless states on the surface of magnetic topological insulators. Physical Review B 102, 245136, doi:10.1103/PhysRevB.102.245136 (2020).
3. Ruie Lu, Hongyi Sun, Shiv Kumar, Yuan Wang, Mingqiang Gu, Meng Zeng, Yu-Jie Hao, Jiayu Li, Jifeng Shao, Xiao-Ming Ma, Zhanyang Hao, Ke Zhang, Wumiti Mansuer, Jiawei Mei, Yue Zhao, Cai Liu, Ke Deng, Wen Huang, Bing Shen, Kenya Shimada, Eike F Schwier, Chang Liu, Qihang Liu & Chaoyu Chen. Half-Magnetic Topological Insulator with Magnetization-Induced Dirac Gap at a Selected Surface. Physical Review X 11, 011039, doi:10.1103/PhysRevX.11.011039 (2021).
4. Xiao-Ming Ma, Yufei Zhao, Ke Zhang, Shiv Kumar, Ruie Lu, Jiayu Li, Qiushi Yao, Jifeng Shao, Fuchen Hou, Xuefeng Wu, Meng Zeng, Yu-Jie Hao, Zhanyang Hao, Yuan Wang, Xiang-Rui Liu, Huiwen Shen, Hongyi Sun, Jiawei Mei, Koji Miyamoto, Taichi Okuda, Masashi Arita, Eike F. Schwier, Kenya Shimada, Ke Deng, Cai Liu, Junhao Lin, Yue Zhao, Chaoyu Chen, Qihang Liu & Chang Liu. Realization of a tunable surface Dirac gap in Sb-doped MnBi2Te4. Physical Review B 103, L121112, doi:10.1103/PhysRevB.103.L121112 (2021).

Experimental Evidence of Six-Fold Degenerate Fermions in $PdSb_2$

Jayita Nayak *et al.*

Max Planck Institute for Chemical Physics of Solids, Nöthnitzer Str. 40, 01187 Dresden, Germany

Keywords: Electronic structure, Multifold degenerate Fermions, Sextuple point

Condensed matter systems can exhibit quasiparticle excitations which mimic the wavefunctions of exotic fermions predicted in high energy physics. For example, Dirac and Weyl fermions exist as low energy electronic excitations of several semimetals near the Dirac points and Weyl points. Most interestingly, condensed matter systems can also realize novel fermions which have no counterpart in high energy physics because the former do not need to follow certain symmetries which are mandatory for the latter. Bradlyn *et al.* discovered that one can find threefold, sixfold, or eightfold degenerate symmetry protected points in many compounds [1]. While the threefold points can be realized in both nonsymmorphic [1,2] and symmorphic crystal structures [2], nonsymmorphic operations are essential for stabilizing sixfold and eightfold degenerate points. **The present study shows that the nonsymmorphic compound $PdSb_2$ hosts six-component fermions or sextuplets.** The sextuple points have been recently observed experimentally in the chiral compound CoSi, RhSi, and AlPt in the space group $P2_13$ (198) [3–5]. However, the latter study was mainly focused on establishing the existence of surface Fermi arcs, which are a consequence of the large Chern number associated with the sixfold crossings in this space group. By contrast, here we show for the first time the existence of sextuple points that have a vanishing Chern number and are therefore expected to show no surface Fermi arcs [6].

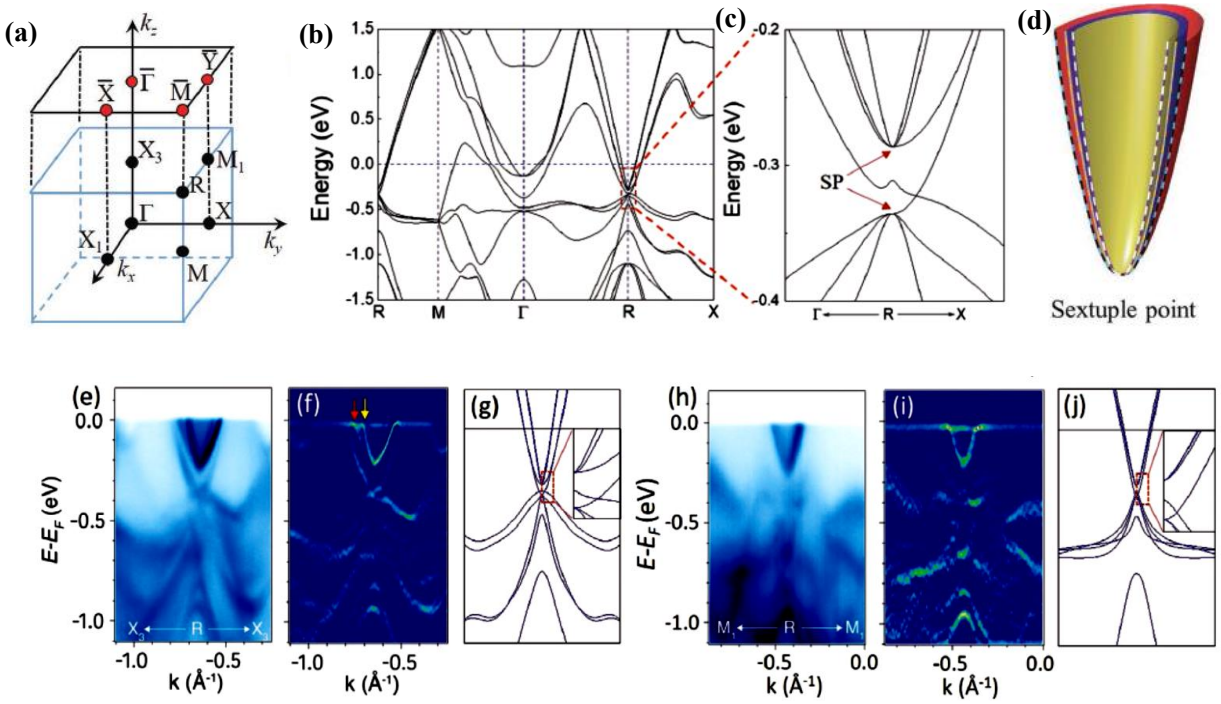

FIGURE 1. a) 3D bulk Brillouin zone (BZ) and (001) surface BZ with the high symmetry points highlighted. b) Calculated band structure along *R*–*M*–Γ–*R*–*X*. Two sextuple points (SPs) are observed at the *R* point at −0.286 & −0.334 eV below the Fermi level, indicated by red arrows in the magnified image on the right (c). Schematic representation of sextuple points (d). e) Measured band dispersion along the X_3−*R*−X_3 direction, at the photon energy 65 eV. f) The corresponding curvature intensity plot. g) Calculated band structure along X_3−*R*−X_3. Inset shows the magnified view near the sextuple point. h–j) ARPES intensity plot, the corresponding curvature intensity plot, and the calculated band structure along M_1−*R*−M_1.

REFERENCES

1. B. Bradlyn, J. Cano, Z. Wang, M. G. Vergniory, C. Felser, R. J. Cava, B. A. Bernevig, *Science* **2016**, *353*, aaf5037.
2. Z. Zhu, G. W. Winkler, Q. Wu, J. Li, A. A. Soluyanov, *Phys. Rev. X* ***6,*** 031003 (2016).
3. D. S. Sanchez, I. Belopolski, T. A. Cochran, X. Xu, J.-X. Yin, G. Chang, W. Xie, K. Manna, V. Süß, C.-Y. Huang, N. Alidoust, D. Multer, S. S. Zhang, N. Shumiya, X. Wang, G.-Q. Wang, T.-R. Chang, C. Felser, S.-Y. Xu, S. Jia, H. Lin, M. Z. Hasan, *Nature* ***567***, 500 (2019).
4. Z. Rao, H. Li, T. Zhang, S. Tian, C. Li, B. Fu, C. Tang, L. Wang, Z. Li, W. Fan, J. Li, Y. Huang, Z. Liu, Y. Long, C. Fang, H. Weng, Y. Shi, H. Lei, Y. Sun, T. Qian, H. Ding, *Nature* ***567***, 496 (2019).
5. N. B. M. Schröter, D. Pei, M. G. Vergniory, Y. Sun, K. Manna, F. de Juan, J. A. Krieger, V. Süss, M. Schmidt, P. Dudin, B. Bradlyn, T. K. Kim, T. Schmitt, C. Cacho, C. Felser, V. N. Strocov, Y. Chen, *Nat. Phys.* ***15***, 759 (2019).
6. Nitesh Kumar, Mengyu Yao, Jayita Nayak, Maia G. Vergniory, Jörn Bannies, Zhijun Wang, Niels B. M. Schröter, Vladimir N. Strocov, Lukas Müchler, Wujun Shi, Emile D. L. Rienks, J. L. Mañes, Chandra Shekhar, Stuart S. P. Parkin, Jörg Fink, Gerhard H. Fecher, Yan Sun, B. Andrei Bernevig, and Claudia Felser, *Adv. Mater.* **1906046,** pp 1-6 (2020).

Angle-dependent XMCD as a Probe of Anisotropic Spin-density Distribution

Goro Shibata[a]

[a]*Department of Applied Physics, Tokyo University of Science, 6-3-1 Niijuku, Katsushika-ku, Tokyo 125-8585, Japan*

Keywords: X-ray magnetic circular dichroism, Magnetic anisotropy, Thin films, Anisotropic charge distribution, Orbital degree of freedom, Magnetic dipole moment

Magnetic thin films often exhibit magnetic anisotropy due to epitaxial strain, surface and interfacial effects, lowered dimensionality, and so on. In general, magnetic anisotropy arises from the combined effects of anisotropic electronic structure and spin-orbit interaction (SOI). Understanding the detailed mechanism of the magnetic anisotropy in ferromagnetic thin films and controlling it have been one of the major research issues both from scientific and technological points of view. Since the electronic structure of magnetic thin films can be highly anisotropic, soft x-ray spectroscopy, including, x-ray absorption spectroscopy (XAS) and x-ray magnetic circular/linear dichroism (XMCD/XMLD), with varying incident angles and magnetic-field angles will give new insights into the magnetic anisotropy of thin films.

We have developed the 'vector-magnet' apparatus for XMCD and XMLD measurements, in which the direction of the magnetic field can be varied two-dimensionally [1]. It has been theoretically predicted that the "magnetic dipole moment" M_{T} or "electric quadrupole moment" Q_{zz}, which represent the anisotropy of spin/charge density distribution (i.e. elongation or shrinkage of electron orbitals of magnetic ions), can be deduced through such angle-dependent XMCD and XMCD measurements [2,3]. In this talk, I will introduce our recent studies on the magnetic anisotropy of $La_{1-x}Sr_xMnO_3$ (LSMO) thin films via the angle-dependent XMCD and XMLD measurements [4,5]. LSMO is a material which shows ferromagnetic metallicity in the widest ranges of hole concentration x and has highest Curie temperature above the room temperature among colossal-magnetoresistive perovskite manganites. From the angle-dependent XMCD experiments [4], it has been demonstrated that the anisotropy of the spin-density distribution of Mn 3*d* electrons changes depending on the epitaxial strain and that it is correlated with the change of strain-induced magnetic anisotropy [6]. From the XMLD experiments [5], changes in the charge-density anisotropy of Mn 3*d* electrons induced by the spin polarization has been observed, which can be understood as the inverse process of the strain-induced magnetic anisotropy. These angle-dependent XMCD and XMLD measurements will pave a new way for elucidating the origin of magnetic anisotropy in various transition-metal thin films by directly probing the anisotropic electronic structure.

REFERENCES

1. M. Furuse *et al.*, *IEEE Trans. Appl. Supercond.* **23**, 4100704-1--4 (2013).
2. J. Stöhr and H. König, Phys. Rev. Lett. **75**, 3748--3751 (1995).
3. H. A. Dürr and G. van der Laan, Phys. Rev. B **54**, R760--R763 (1996).
4. G. Shibata *et al.*, *npj Quantum Mater.* **3**, 3-1--6 (2018).
5. G. Shibata *et al.*, *J. Phys. Soc. Jpn.* **87**, 114713-1--5 (2018).
6. G. van der Laan, *J. Phys. Condens. Matter* **10**, 3239--3253 (1998).

X-ray Magnetic Circular Dichroism in a Chiral Antiferromagnet

Yuichi Yamasaki

[a] *National Institute for Materials Science*

Keywords: X-ray magnetic circular dichroism, antiferromagnet

X-ray magnetic circular dichroism (XMCD) has become a versatile technique to ferro- and ferrimagnetic magnetic materials. The technique enables us to extract the expectation values of the element-specific spin and orbital moments. In contrast, it has been generally believed that XMCD does not occur in antiferromagnets which do not have net magnetization.

A chiral magnet Mn_3Sn exhibits a coplanar 120° antiferromagnetic (AFM) order on breathing Kagomé-type Mn network, which breaks the time reversal symmetry and allows the anomalous Hall effect [1] and the magneto-optical Kerr effect (MOKE) [2] even though the magnetic moments almost cancel each other. We have theoretically investigated a possibility of x-ray magnetic circular dichroism (XMCD) in the AFM state of Mn_3Sn [3]. The spin operator term in XMCD, the so-called S_z term, should be negligibly small as well as the net magnetization. However, it is clarified that the anisotropic magnetic dipole (AMD) operator term, the so-called T_z term, remains uncancelled in the AFM order and is linked to the augmented (cluster) magnetic octupole (see Figure). Based on this prediction, XMCD experiments were performed on bulk crystals of Mn_3Sn. As a result, we succeeded in observing XMCD at Mn-L absorption edge and demonstrated that the XMCD signal is purely coming from the T_z tern by its magnetic field and incident angle dependence and comparing with theoretical calculations of the spectrum [4].

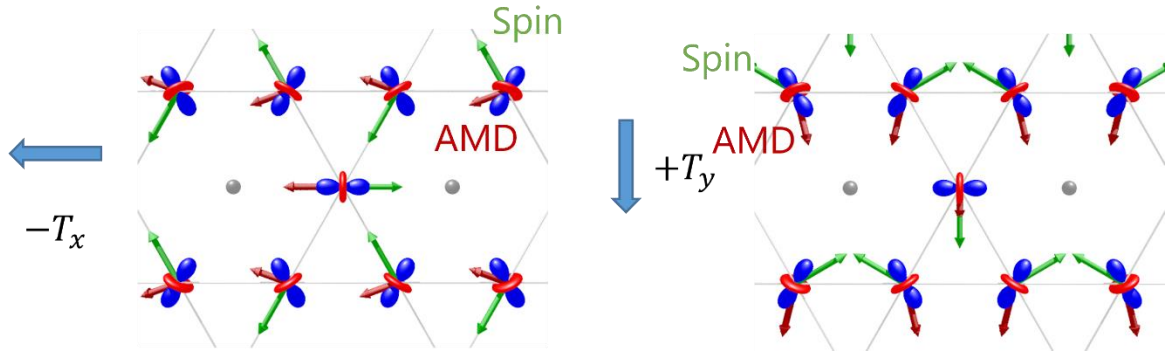

REFERENCES

1. S. Nakatsuji, N. Kiyohara, and T. Higo, Nature 527, 212 (2015).
2. T. Higo, et al., Nat. Photonics 12, 73 (2018).
3. Y. Yamasaki, H. Nakao, T. Arima, J. Phys. Soc. Jpn. 89, 083703 (2020)
4. M. Kimata, Y. Yamasaki, Tetsuya Nakamura, *et al*., Nat. Commun. 12, 5582 (2021)

Spin-Resolved Photoemission of Heusler-Type Weyl Ferromagnet Films

Kazuki Sumida[a]

[a]*Materials Sciences Research Center, Japan Atomic Energy Agency, Hyogo 679-5148, Japan*

Keywords: Spin-resolved ARPES, Heusler alloy, Weyl ferromagnet, Anomalous Nernst effect, Berry curvature.

When electric and thermal currents flow through a ferromagnet, an electric field emerges orthogonally to the current path [Fig. 1(a)]. The two effects are, respectively, called the anomalous Hall (AHE) and Nernst (ANE) effects and are exploited as operating mechanisms in various novel applications. The associated transverse voltage of the electric field is empirically proportional to its spontaneous magnetization. In contrast to the general belief, recent discoveries of both large AHE and ANE, which do not scale with magnetization, have elicited great surprise. In particular, the observed ANE thermopower and AHE conductivity of single crystalline bulk Co_2MnGa and Co_2MnAl are an order of magnitude larger than those of other ferromagnets with similar magnetizations [1,2,3]. These transverse properties are postulated to arise from a Berry curvature emerging within band structures near the Fermi energy (E_F).

Topologically non-trivial Weyl semimetals possessing massless fermions characterized by zero-gap and linear band dispersions are promising candidates featuring a large Berry curvature. Weyl fermions in solids can be realized in materials that break inversion symmetry or time-reversal symmetry. With the breaking of such symmetries, Weyl nodes appear as pairs in momentum space and act as magnetic monopoles with positive and negative chiralities. To date, Weyl fermions have been verified in experiments in non-centrosymmetric (e.g., TaAs-family) and magnetic materials (e.g., Mn_3Sn) through angle-resolved photoelectron spectroscopy (ARPES) and magneto-transport measurements [4,5].

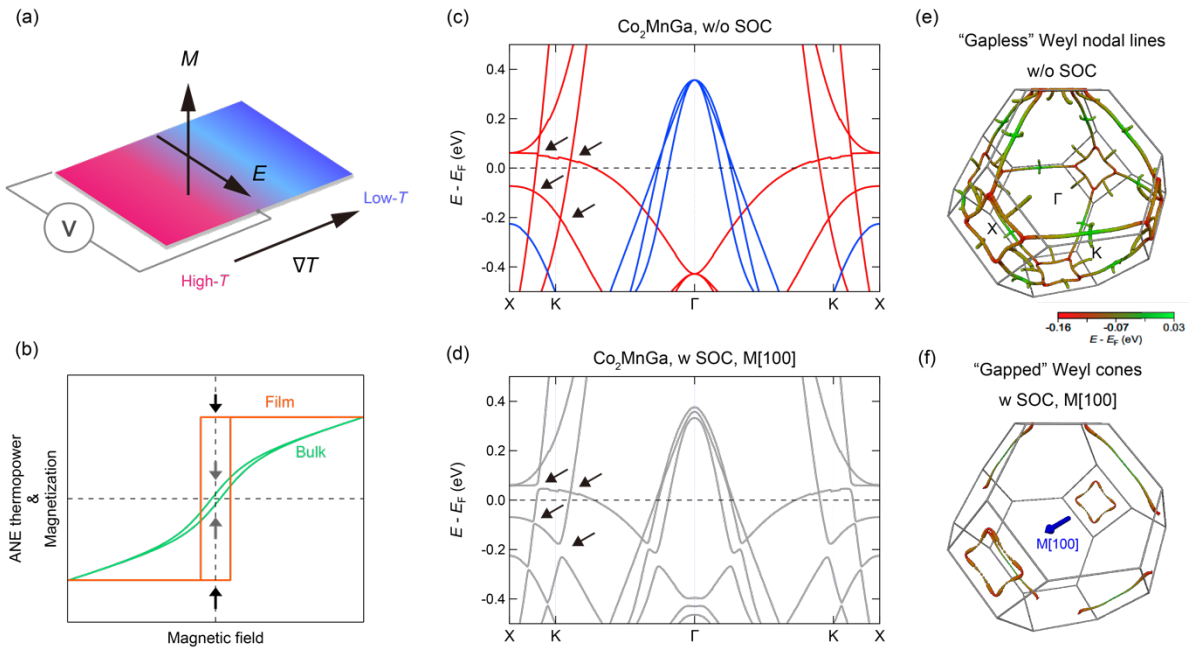

FIGURE 1. Schematic illustrations of (a) the ANE and (b) the ANE thermopower and magnetization of Heusler alloy in bulk and film forms. Black and gray arrows indicate the remanence magnetization. (c,d) Calculated band structures of Co_2MnGa Heusler alloy without and with spin-orbit coupling (SOC). Red and blue colors correspond to the majority and minority spin. (e,f) Three-dimensional view of the Weyl nodal lines of Co_2MnGa without and with SOC. Color corresponds to the location of the Weyl node. The blue arrow in (f) indicates the direction of magnetization.

Recently, Co_2MnGa and Co_2MnAl Heusler alloys have also been theoretically predicted to be a ferromagnetic Weyl semimetal [6] and has been experimentally demonstrated in the bulk form to exhibit large anomalous transport properties under an external magnetic field [1,2,3]. The nature of this highly symmetric crystal creates mirror-symmetry-protected Weyl nodal lines in the band structure as encountered by theory [Figs. 1(c) and 1(e)] and experiments [7]. However, the nodal lines lead to vanishing Berry curvature when integrated over the whole Brillouin zone and cannot explain the observed phenomena. One way to obtain a large Berry curvature is to gap out their nodal lines using remanent magnetization or an external magnetic field (specifically, to break the mirror symmetry) [Figs. 1(d) and 1(f)]. Yet, the experimental evidence for broken mirror symmetry was not provided by the recent ARPES measurement on bulk Co_2MnGa crystal because the remanent magnetization was negligible [Fig. 1(b)] as applying external magnetic fields is not permitted in this measurement. For practical applications in which zero-field operation and gigantic outputs are a requirement, it is thus indispensable to truly understand the band structure responsible for the anomalous transport properties in films with full remanent magnetization.

In this talk, I show the spin-polarized band structure and anomalous transport properties of ferromagnetic Co_2MnGa thin films [8]. Growth of high-quality thin films possessing full remanent magnetization and in situ spin-resolved ARPES (SARPES) measurements permit access to their non-trivial band structures modified by the broken mirror symmetry. We observed spin-polarized Weyl cones located mostly at a Lifshitz quantum critical point and a flat band of surface states [Fig. 2]. Furthermore, when the energy associated with the "massive" Weyl cone approaches E_F, the AHE and ANE conductivities systematically increase as the electron number rises. In particular, the ANE reaches thermopower of ~6.2 μV/K at room temperature, which is the highest amongst magnetic films to the best of our knowledge. In addition, I also present the spin-polarized band structure of the quaternary $Co_2Mn(Al,Si)$ Heusler film. We succeeded in doping electrons about 350 meV in the Weyl ferromagnet Co_2MnAl by Si substitution and revealed that the spin-polarized multiple Weyl cones and half-metallic gap coexist in the bulk electronic structure [9].

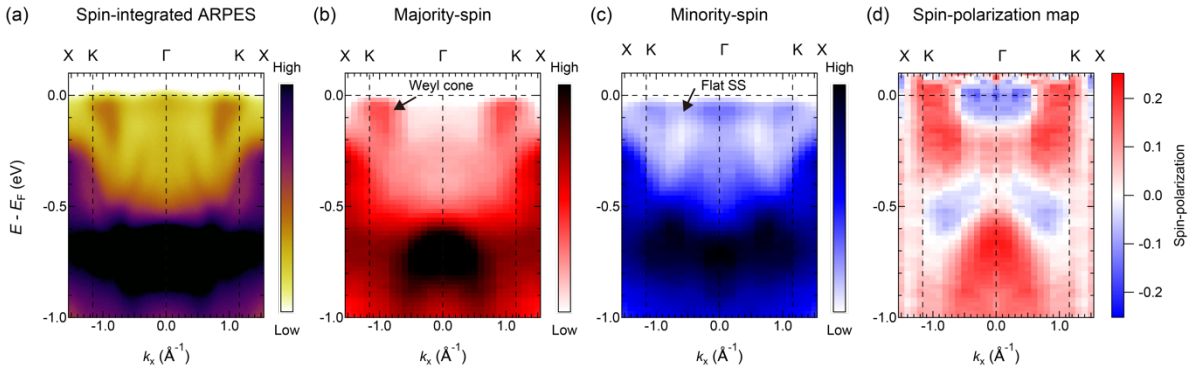

FIGURE 2. (a) Spin-integrated ARPES image of Co-rich Co_2MnGa film along Γ-K-X line recorded at 80 eV with *p*-polarized light. (b,c) SARPES images of the majority and minority spin states. (d) Spin-polarization map. ARPES and SARPES images are symmetrized with respect to the Γ point.

REFERENCES

1. A. Sakai *et al*., *Giant anomalous Nernst effect and quantum-critical scaling in a ferromagnetic semimetal*, Nat. Phys. **14**, 1119 (2018).
2. S. N. Guin *et al*., *Anomalous Nernst effect beyond the magnetization scaling relation in the ferromagnetic Heusler compound Co_2MnGa*, NPG Asia Materials **11**, 16 (2019).
3. P. Li *et al*., *Giant room temperature anomalous Hall effect and tunable topology in a ferromagnetic topological semimetal Co_2MnAl*, Nat. Phys. **11**, 3476 (2020).
4. S.-Y. Xu *et al*., *Discovery of a Weyl fermion semimetal and topological Fermi arcs*, Science **349**, 613 (2015).
5. K. Kuroda *et al*., *Evidence for magnetic Weyl fermions in a correlated metal*, Nat. Mater. **16**, 1090 (2017).
6. J. Kuebler and C. Felser, *Weyl points in the ferromagnetic Heusler compound Co_2MnAl*, EPL **114**, 47005 (2016).
7. I. Belopolski *et al*., *Discovery of topological Weyl fermion lines and drumhead surface states in a room temperature magnet*, Science **365**, 1278 (2019).
8. K. Sumida *et al*., *Spin-polarized Weyl cones and giant anomalous Nernst effect in ferromagnetic Heusler films*, Commun. Mater. **1**, 89 (2020).
9. K. Sumida *et al*., *in preparation.*

Chirality-Induced Spin Polarization in Chiral Crystals

Yoshihiko Togawa

Department of Physics and Electronics, Osaka Prefecture University, Sakai, Osaka 599-8531 Japan

Keywords: Chirality, Spin polarization, Macroscopic spin response

A role of chirality in materials is discussed in terms of an emergence of macroscopic spin response, being inspired by recent works on chiral magnetism and chirality-induced spin polarization. These viewpoints may bring us to a new frontier of chiral material science. In this connection, we will focus the experimental findings that chiral materials exhibit a spin-polarized state when the charge current is injected into them [1-4]. A spin-polarized transport occurs in a linear regime of the current-voltage characteristics. Importantly, a robust protection of the spin polarization enables a nonlocal spin transport over micrometers or longer. A comprehensive understanding of these nontrivial spin response remains an important issue and may clarify the interplay between structural and dynamical chirality. This work was done in collaboration with the laboratory members in OPU. I sincerely appreciate their great efforts on performing experiments.

REFERENCES

1. A. Inui, R. Aoki, Y. Nishiue, K. Shiota, Y. Kousaka, H. Shishido, D. Hirobe, M. Suda, J. Ohe, J. Kishine, H. M. Yamamoto, Y. Togawa, *Physical Review Letters* **124**, 166602 (2020).
2. Y. Nabei, D. Hirobe, Y. Shimamoto, K. Shiota, A. Inui, Y. Kousaka, Y. Togawa, and H. M. Yamamoto, *Applied Physics Letters* **117**, 052408 (2020).
3. K. Shiota, A. Inui, Y. Hosaka, R. Amano, Y. Onuki, M. Hedo, T. Nakama, D. Hirobe, J. Ohe, J. Kishine, H. M. Yamamoto, H. Shishido, and Y. Togawa, *Physical Review Letters* **127**, 126602 (2021).
4. H. Shishido, R. Sakai, Y. Hosaka, and Y. Togawa, *Applied Physics Letters* **119**, 182403 (2021).

Construction and Operation of Superconducting Bending Magnets in Aichi-SR

Yoshifumi Takashima[a,b]

[a] *Synchrotron Radiation Research Center, Nagoya University, Furo-cho, Chikusa-ku, Nagoya City, Aichi, 464-8601, Japan*
[b] *Aichi Synchrotron Radiation Center, Minamiyamaguchi-cho 250-3, Seto City, Aichi, 489-0965, Japan*

Keywords: Superconducting magnet, Storage ring.

Aichi Synchrotron Radiation Center (Aichi-SR) started public use of synchrotron radiation in March 2013 [1]. The facility is operated mainly by Aichi Science & Technology Foundation and is supported by universities, Aichi Prefecture, and industry. At present, 11 beamlines are in operation, including one each from industry and university, and a new beamline for the industry is under construction.

Accelerators of the Aichi-SR consist of a 50 MeV linear accelerator, a 1.2 GeV booster synchrotron, and a 1.2 GeV electron storage ring of a 72 m circumference [2-5]. A notable feature of the Aichi-SR accelerator is that it uses superconducting bending magnets (superbends) to supply synchrotron radiation to multiple beamlines with energies exceeding 10 keV, despite the relatively low electron energy of 1.2 GeV [6]. The magnetic lattice configuration is the four-fold symmetry of triple-bend cell. In the unit cell of the three bending magnets, the two at both ends are normal-conducting magnets with a magnetic field of 1.4 T and a bending angle of 39°, and the one in the center is a superconducting magnet with a peak magnetic field of 5 T and a bending angle of 12°. Figure 1 and Figure 2 show the layout of the accelerators, and the flux of synchrotron radiation from the superbend and the normal-conducting bending magnet at Aichi-SR.

For the cooling of the superbends, a small 4K-GM type refrigerator is placed one by one in each superbend, and the superconducting coils are cooled directly. The direct cooling method, which does not use liquid helium, is advantageous not only in terms of cost but also in terms of ease of maintenance, such as handling in case of quenching. Figure 3 shows a photo of the suberbends.

The refrigerators of the superbends need to be maintained after 10,000 hours of operation. Immediately after the refrigerator was replaced, the temperature rose to about 60 K, but it reached below 3.6 K in about 24 hours. The maintenance of the refrigerators is done once a year, and in all cases since the construction of Aichi-SR, the coil temperature returns to below 3.6 K after the maintenance.

The superbends of the Aichi-SR have had some trouble with the refrigerators, but no problem with the magnets themselves and are now operating smoothly.

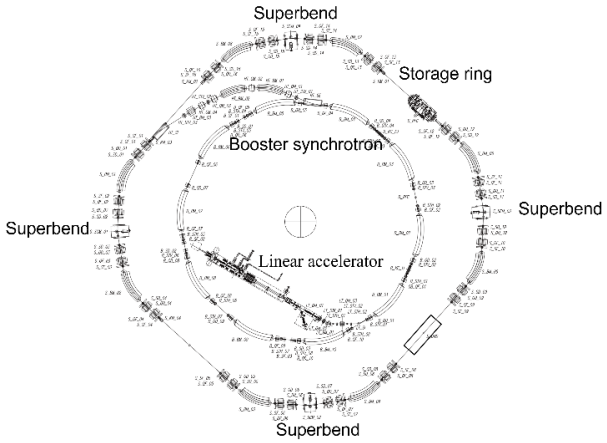

FIGURE 1. Layout of Aichi-SR accelerators.

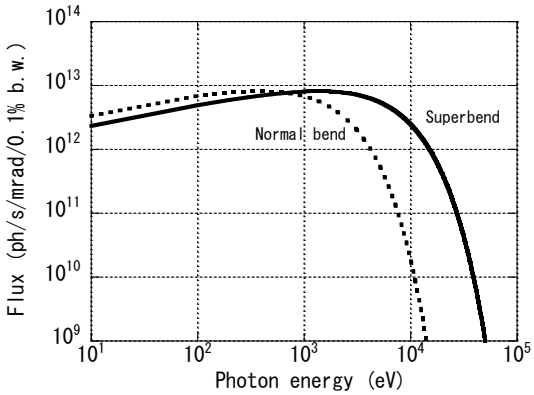

FIGURE 2. Flux of synchrotron radiation from the superconducting bending magnet (Superbend) and the normal-conducting bending magnet (normal bend).

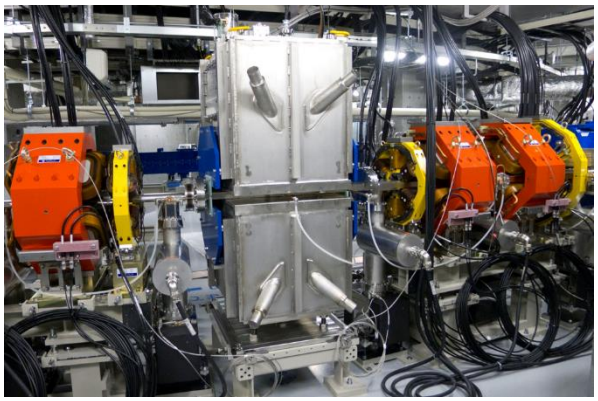

FIGURE 3. Superconducting bending magnet of Aichi-SR.

ACKNOWLEDGMENT

I want to great thank Prof. M. Katoh of HiSOR, Prof. M. Hosaka of USTC, and Associate Prof. N. Yamamoto of KEK for their tremendous support in the basic design, commissioning, and machine study of the Aichi-SR accelerators. In the daily operation of the Aichi-SR accelerators, I am very grateful for the contribution of the Aichi-SR accelerator division staff. Furthermore, I greatly appreciate Toshiba Corporation for their significant contribution to constructing the accelerators, including the superbends. I am also very grateful to Dr. M. Torikoshi of NIRS for allowing us to borrow their superconducting wiggler test machine.

REFERENCES

1. https://www.aichisr.jp/index.html
2. A. Mochihashi et al., "PRESENT STATUS OF ACCELERATORS IN AICHI SYNCHROTRON RADIATION CENTER", Proceedings of IPAC2017, Copenhagen, Denmark, 2017, pp. 2691-2693.
3. Y. Takashima et al., "PRESENT STATUS OF ACCELERATORS IN AICHI SYNCHROTRON RADIATION CENTER", Proceedings of IPAC2016, Busan, Korea,2016, pp. 2877-2879.
4. N. Yamamoto et al., “ACCELERATORS OF THE CENTRAL JAPAN SYNCHROTRON RADIATION FACILITY PROJECT (II)”, Proceedings of IPAC2011, San Sebastián, Spain, 2011, pp. 2987-2989.
5. N. Yamamoto et al., “ACCELERATORS OF THE CENTRAL JAPAN SYNCHROTRON RADIATION FACILITY PROJECT”, Proceedings of IPAC2010, Kyoto, Japan, 2010, pp. 2567-2569.
6. M. Hosaka et al., "PRESENT STATUS OF SUPER-CONDUCTIVE BENDING MAGNETS AT AICHI SR", Proceedings of the 10th Annual Meeting of Particle Accelerator Society of Japan, Nagoya, Japan, 2013, pp. 461-464.

Recent Results from Design Study on HiSOR-2

Masahiro Katoh[a,b]

[a]*Hiroshima University,1-3-1 Kagamiyama, Higashi-Hiroshima 739-8526, Japan*
[b]*Institute for Molecular Science, National Institutes of Natural Sciences, 38 Nishigo-Naka, Myodaiji, Okazaki, 444-8585, Japan*

Keywords: Synchrotron light source, electron storage ring.

HiSOR, a low energy and compact synchrotron light source in Hiroshima University, has two straight sections and is capable of producing high-brightness light in the vacuum ultraviolet range from two undulators. It has two normal conducting bending magnets, which have high field strength of 2.7 T and are capable of producing synchrotron radiation in a wide range including tender X-rays even with the low electron energy, 700MeV. Since no major upgrade has been made on the accelerator since its construction in 90's, the operation of HiSOR is well established and stable in these years. On the other hand, after 25 years from its construction, the hardware has been being aged and its competitiveness in terms of light source performance are being lowered among the newly constructed light sources over the world. Some of the light sources in Japan, such as Photon Factory [1] or UVSOR [2], have been upgraded with some major modifications of the hardware. SPring-8 also has an upgrade plan [3]. In case of HiSOR, it was designed and manufactured by a single company. It has a rational design without redundancy. Therefore, it is difficult to make a major modification to improve the performance or introduce new technologies to the present machine. Therefore, we have been designing a completely new ring for the future plan of the facility [4].

The latest version of the design [4] is as follows; the circumference is about 50 m and the electron energy is 500 MeV. The emittance, which is the most important parameter to achieve high brightness, is around 10nm, which is smaller by two orders of magnitudes than the present value, 400nm. It has six straight sections and four of them can be used for installing undulators. It would have a full energy injector for the top-up operation, which consists of a linear accelerator and a booster synchrotron. We believe such a new facility is ideal for further developing the research activities which have been carried out at HiSOR for over twenty years. On the other hand, this plan requires a significant budget, which may not be easy to be approved. In addition, the feasibility of this plan also depends largely on the trends of the future plans of other synchrotron light sources in Japan. Therefore, as leaving this plan as one candidate, we have started designing alternative plan, which might be realized with less budget.

To reduce the construction cost as keeping the high performance as possible, we have designed a compact storage ring as shown in Fig. 1. The circumference is about 30 m and the electron energy is 500 MeV. The emittance is 17 nm. The ring has six 2.2 m straight sections, four of which can be used for undulators. The diameter of the ring is almost same as the major axis of the present HiSOR ring. This compactness may reduce the construction cost of the accelerator. One interesting possibility is to install this ring in the present experimental hall. If this is the case, the total construction cost would be reduced significantly.

The magnetic lattice of the new design is very simple, which may be realized with combined-function magnets. The bending magnets should produce quadrupole and sextupole fields and the quadrupole magnets sextupole fields as well as dipole fields for beam steering. It was proved that, after compensating the linear chromaticity with two families of sextupoles, the dynamic aperture is sufficiently large. The beam injection may be realized with a pulsed multipole magnet [5].

In adding to making the storage ring compact, one interesting possibility to further reduce the construction cost is utilizing the present HiSOR storage ring as an injector. We can find several examples of such utilization of older storage rings as injectors for new rings, even though they were not capable of rapid cycling of acceleration [6, 7]. In our case, the electron beam from the existing 150 MeV microtron is injected to the present HiSOR ring and is accelerated up to 500 MeV, then is extracted and transferred to the new ring. Since it is expected that the construction cost of a full energy injector is almost as high as that of the new storage ring, the recycling of old accelerator is effective to reduce the cost. An interesting possibility

for further reduction of the cost is moving the present HiSOR to the injector room and constructing new storage ring in the present storage ring room.

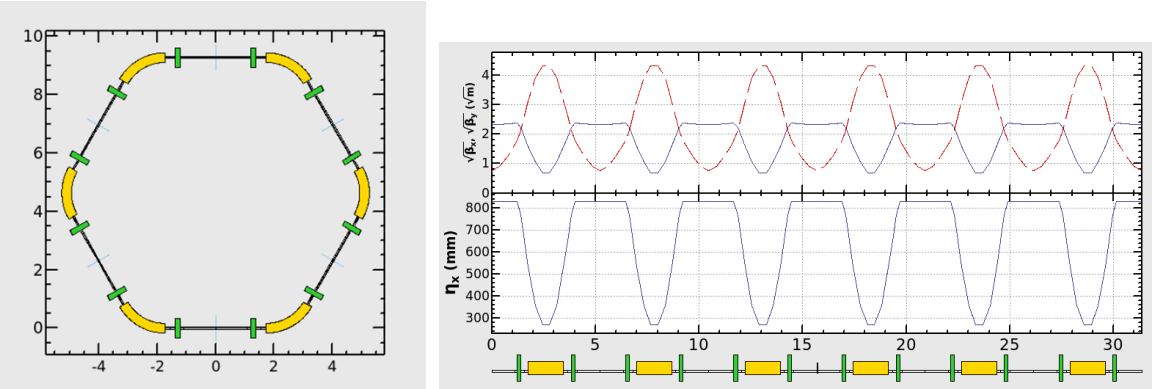

FIGURE 1. Magnetic lattice (left) and optical functions (right) of the new lattice design for HiSOR-2.

The typical synchrotron radiation spectra are shown in Fig. 2. For comparison with the present ring, we calculated the spectra for the undulators which are currently operational in the present HiSOR. The brightness is improved by more than one order of magnitudes. Since the electron energy of HiSOR-2 is lower than the present value, the spectral ranges shift to the lower photon energy. Shorter period undulators may be installed to cover the higher energy range.

In the present HiSOR, the photon energy range up to the tender X-rays is covered with the bending radiation from the high field normal conducting bending magnets. In HiSOR-2, the bending magnets will be normal conducting and have ordinary field strengths such as around 1 T. In addition, the electron energy is lower. Therefore, the bending radiation cannot cover the X-ray range. If there are strong demands for the X-rays, one idea is to replace two or three bending magnets with superconducting ones of 5 T. In this case, even with the lower electron energy, the ring can cover almost same photon energy range. The electron beam optics should be designed carefully not enlarging the emittance so much.

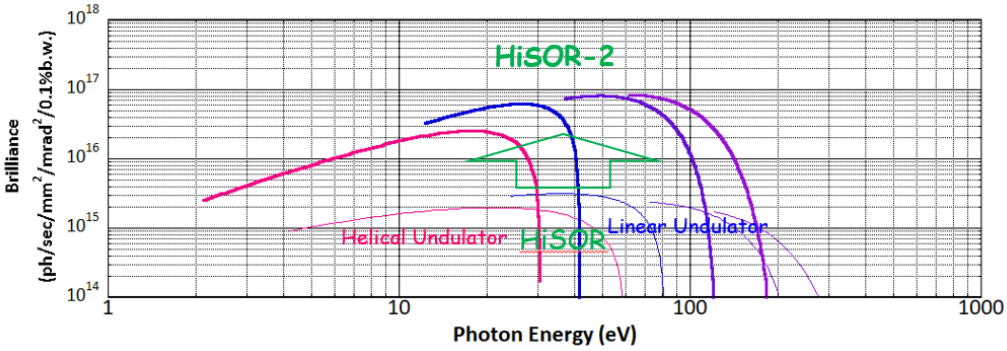

FIGURE 1. Synchrotron radiation spectra on the alternative design of HiSOR-2. The undulator parameters are same as the present HiSOR.

REFERENCES

1. M. Katoh *et al*., *J. SYNCHROTRON RAD.* 5(3) 366 - 368 (1998).
2. M. Katoh *et al*., *Nucl. Instr. Meth. A*. 467, 68 - 71 (2001).
3. http://rsc.riken.jp/pdf/SPring-8-II.pdf.
4. S. Matsuba *et al., J. Phys. Conf. Ser*. 1350 012015-1~5 (2019).
5. K. Hirata *et al*., HiSOR Activity Report 2019, 12 (2020), .
6. G. LeBlanc *et al*., Proc. EPAC'96, 345 (1996).
7. S.P. Møller *et al*., Proc. iPAC2013, 64 (2013).
6. K. Hiramatsu *et al*., HiSOR Activity Report 2020, 11 (2021).

Applications of the Generalized-High Accuracy Universal Polarimeter (G-HAUP) to Solid State Sciences

Toru Asahi[a,b] and Kenta Nakagawa[c]

[a] *Faculty of Science and Engineering, Waseda University, 2-2 Wakamatsu-cho, Shinjuku-ku, Tokyo, 162-8480, Japan.*
[b] *Research Organization for Nano & Life Innovation, Waseda University, 513 Wasedatsurumaki-cho, Shinjuku-ku, Tokyo, 162-0041, Japan.*
[c] *Kanagawa Institute of Industrial Science and Technology (KISTEC), 705-1 Shimo-imaizumi, Ebina, Kanagawa, 243-0435, Japan*

Keywords: Magneto-optics, Faraday rotation, CeF_3 single-crystal, G-HAUP.

The optical study on condensed matters is a powerful tool for investigating spatial symmetry breaking and/or time-reversal symmetry breaking. Optical activity (OA) and circular dichroism (CD) are related to spatial and time-reversal symmetry. Natural OA and CD, which are reciprocal signals, were observed when the spatial symmetry was broken. On the other hand, Faraday rotation and magnetic circular dichroism, which are non-reciprocal signals, were observed when the time-reversal symmetry was broken. [1] Here, we emphasize the consideration of linear birefringence (LB) and linear dichroism (LD) in the measurement of OA and CD in anisotropic crystals. LB and LD are optical anisotropies that denote the difference in refractive indices and absorptions, respectively, between two orthogonally polarized lights in an anisotropic crystal. Schellman *et al.* [2] reported that LB and LD signals are usually 10^3–10^5 times larger in magnitude than OA and CD signals. Therefore, the accurate separation of OA and CD from LB and LD is a challenge. Furthermore, Shindo *et al.* [3] pointed out that optical elements, devices, and detectors installed in polarization modulation spectroscopy cause serious systematic errors and non-negligible artifacts. This critical issue has been widely recognized in the field of chiral science. Many research groups have developed optical measurement theories and polarimeters to overcome this issue. Eventually, OA and CD in the anisotropic condensed matter were successfully measured. In particular, we developed a novel optical apparatus called the generalized-high accuracy universal polarimeter (G-HAUP), which simultaneously measures the wavelength dependences of the OR, CD, LB, and LD in an anisotropic medium. [4–10] Regardless, some researches in the field of magneto-optics neglected optical anisotropies, systematic errors, and artifacts in OA and CD measurements.

This study investigates the wavelength dependences of linear birefringence, linear dichroism, Faraday rotation and magnetic-circular dichroism in a single crystal rare-earth fluoride, namely CeF_3. The subject material selected Faraday rotator in the present study CeF_3 single crystal, is characterized by its wide transparency range (300 nm to 2500 nm) and an outstanding Verdet constant, besides of being uniaxial. Cerium is usually found as a trivalent ion Ce^{3+} in condensed matter. The electronic configuration of Ce^{3+} is $1s^2 2s^2 2p^6$ … $4d^{10} 4f^1 5s^2 5p^6$. Electronic transitions from 4*f* to 5*d* confer the magneto-optical properties observable in the UV-Vis-IR region1. In a previous report, the refractive indices of the ordinary and extraordinary light rays in single crystal CeF_3 at 633 nm were determined as 1.616 and 1.609, respectively. Therefore the LB is 0.007, comparable to that of the α-quartz crystal along its *a* axis. Even at this low order of LB magnitude (10^{-3}), the OR of the crystal cannot be accurately measured by conventional optical apparatuses [16]. Previously, When a sample is subjected to a magnetic field applied parallel/anti-parallel to the light propagation direction, the G-HAUP can measure its FR and Magnetic-CD (MCD). In this study, we measured the wavelength dependences of the FR, MCD and optical anisotropy in CeF_3 single crystal along the optic axis (*c* axis) and perpendicular to the optic axis (*a* axis) with the G-HAUP. [9] A magnetic field parallel/anti-parallel to the light propagation was generated by Nd-Fe-B (NIB) magnets introduced for that purpose.

We prepared a 307-μm thick (001) plate of single-crystal CeF_3 by polishing. In structure, the CeF_3 crystal belongs to the uniaxial and optically inactive crystal point group D_{3d}. Therefore, when the magnetic field is applied parallel to the light propagation direction, FR occurs only along the *c* axis. To apply the magnetic

field parallel or anti-parallel to the light propagation direction, we mounted the sample on a pinhole plate, and sandwiched it between two ring NIB permanent magnets. The wavelength dependences of the Verdet constant along the *c* axis at 25 °C are plotted as black rhombuses in Fig. 1(c). The Verdet constants along the *c* axis were positive over the observed wavelength region, indicating that the right-handed circularly-polarized light propagates faster than its left-handed counterpart.

We then prepared a 58.0-μm thick (100) plate sample of single-crystal CeF_3 by polishing. Before measuring the magneto-optical properties, we determined the wavelength dependences of the LB, LD, OR and CD along the *a* axis in the absence of the magnetic field at 25 °C (blue rhombuses in Fig. 1). The LB along this axis was of the same order of magnitude as the LB of α-quartz crystal (Fig. 1(a)). However, the LDs were almost zero over the wavelength region (Fig. 1(b)). This result is consistent with the UV-Vis spectrum, which exhibits no significant absorption above 282 nm.

Then, the wavelength dependences of the LB, LD, FR, and MCD along the *a* axis under a magnetic field parallel to the light propagation direction at 25 °C were measured (red rhombuses in Fig. 1). In general, reversing the magnetic field direction inverted the signs of FR and MCD. Therefore, in order to obtain accurate spectra, we applied the magnetic field anti-parallel to the light propagation direction, re-measured the wavelength dependences, and averaged the absolute magnitudes of both sets of measurements. The values of LB and LD hardly changed with and without the magnetic field (Fig. 1(a,b)). The Verdet constants along the *a* axis were positive throughout the wavelength region (Fig. 1(c)).

In conclusion, the wavelength dependences of LB, LD, FR and MCD were investigated along the *a* and *c* axes of single crystal CeF_3 under an applied magnetic field. These measurements were successfully collected by the G-HAUP equipped with NIB magnets. The Verdet constants along the *c* and *a* axes were positive and nearly equal in magnitude in the measured wavelength region.

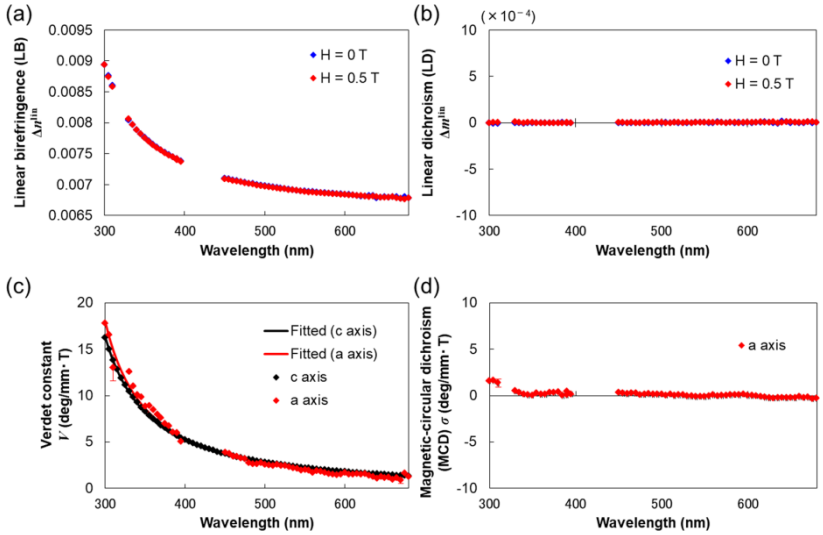

Figure 1. Wavelength dependences of the LB (a), LD (b), Verdet constant (c) and MCD (d) in single-crystal CeF_3 at 25 °C. Reproduced from Ref. [9] with permission from Springer Nature.

REFERENCES

1. L. D. Barron, Molecular Light Scattering and Optical Activity (Cambridge University Press, New York, (2004) 2nd *ed*.
2. J. A. Schellman and H. P. *Jensen, Chem. Rev.* **87**, 1359 (1987).
3. Y. Shindo, M. Nishiro, and S. Maeda, *Biopolymers* **30**, 405 (1990).
4. M. Tanaka, N. Nakamura, H. Koshima, and T. Asahi, *J. Phys. D* **45**, 175303 (2012).
5. K. Nakagawa, H. H. Lovelady, Y. Tanaka, M. Tanaka, M. Yamato, and T. Asahi, *Chem. Commun.* **50**, 15086 (2014).
6. A. Takanabe, M. Tanaka, K. Johmoto, H. Uekusa, T. Mori, H. Koshima, and T. Asahi, *J. Am. Chem. Soc.* **138**, 15066 (2016).
7. K. Ishikawa, Y. Terasawa, M. Tanaka, and T. Asahi, *J. Phys. Chem. Solids* **104**, 257 (2017).
8. K. Nakagawa, A. T. Martin, S. M. Nichols, V. L. Murphy, B. Kahr, and T. Asahi, *J. Phys. Chem. C* **121**, 25494 (2017).
9. K. Nakagawa and T. Asahi, *Sci. Rep.* **9**, 18453 (2019).
10. Kun Zhang, M. Matsumoto, K. Nakagawa, A. Matsuda, G. Shino, S. Sato, T. Ikeda, and T. Asahi, *J. Phys. Soc. Jpn.* **90**, 113702 (2021)

Exploring active structures of DNA repair protein XRCC4 using CD and SAXS

Akinari Yokoya[a,b], Kai Nishikubo[b,a] and Maho Hasegawa[b,a]

[a]*National Institutes for Quantum Science and Technology, Institute for Quantum Life Science, 2-4 Shirakata, Tokai, Ibaraki 319-1106, Japan*
[b]*Graduate School of Science and Engineering, Ibaraki University, 2-1-1, Bunkyo, Mito 310-8512, Japan*

Keywords: DNA double strand breaks, DNA repair, XRCC4, CD, SAXS, Intrinsically disordered protein.

INTRODUCTION

Ionizing radiation often produces DNA double strand breaks (DSBs). To prevent serious genetic effects from the genome damage, living cells promptly repair DSBs through several pathways. Non-homologous end joining (NHEJ) repair, which is one of the major processes, involves various proteins to rejoin separated DNA ends. XRCC4, a key player of NHEJ, constitutes a polymeric platform of the repair. Normal homodimer formation is thought to change to multimerization by post transcriptional modifications, such as phosphorylation of serine residues, by the certain kinases. So far, protein crystallography was applied to a single crystal of C-terminal deficient XRCC4. The C-terminal tail possesses five phosphorylation sites but is an intrinsically disordered region preventing it from crystallization. Our goal is to elucidate the structural character of dimer and multimer of the full length XRCC4. Two synchrotron analysis methods, namely VUC-circular dichroism (CD) and small-angle X-ray scattering (SAXS) were applied.

EXPERIMENTALS

Purification of XRCC4

To express full-length human XRCC4 (336 amino acids) linked with 6 histidine residues (HisTag), XRCC4 cDNA was obtained from human leukemia cells and inserted into the pET21d plasmid vector. The plasmid was introduced into *E. coli* cells (BL21DE3 Gold) and XRCC4 expression was induced by adding isopropyl β-D-1-thiogalactopyranoside (IPTG) to the culture medium. Using a HisTrap column, XRCC4 was extracted from harvested bacterial cells after homogenizing. The protein was eluted from the column with a buffer containing imidazole (200 mM). XRCC4 dimers were separated from its multimers by gel filtration chromatography. The agarose gel electrophoresis analysis suggested that the multimers inevitably contained a minimal DNA. We used the multimers for CD and SAXS without further purifications.

To mimic phosphorylation, we produced mutated XRCC4 proteins in which the serine residues, S260, S320, S327 or S328, were substituted with a negatively charged aspartic acid, hereinafter denoted as $XRCC4^{S260D}$, $XRCC4^{S320D}$, $XRCC4^{S327D}$ or $XRCC4^{S328D}$, respectively. The mutations were introduced in the XRCC4 coding region using a commercial kit. The results of the pseud-phosphorylated proteins were compared with wild type XRCC4 ($XRCC4^{WT}$).

CD measurements at HiSOR

CD spectroscopy was carried out at BL-12 at the Hiroshima Synchrotron Radiation Center (HiSOR). Protein sample of $XRCC4^{WT}$, $XRCC4^{S260D}$ or $XRCC4^{S327D}$ was dissolved in the sodium phosphate buffer. The sample was encapsulated in a CaF2 cell (path length, 50 μm). CD spectra were measured between 175 and 260 nm at 25°C.

SAXS measurements at the Photon Factory

SAXS was performed at BL-6A at the Photon Factory (PF) in KEK. Each XRCC4 protein sample was dissolved in HEPES buffer at 25°C. The wavelength of X-rays was 1.5 Å (8.3 keV) and the PILATUS-detector (Pixel Apparatus for the SLS) was set at 2500 mm from the sample to detect diffracted X-rays. Volume of the sample cell with a thin polyimide film window was 40 μl and the path length was 1mm.

RESULTS

Secondary structures of XRCC4 determined by CD

The obtained CD spectra of dimer and multimer of the wild type and mutated XRCC4 are shown in Fig. 1. All peak intensities at 190, 210 and 220 nm of the multimer were notably smaller than those of dimer. For

mutated proteins, we also obtained similar CD spectra of their dimer and multimer samples. The secondary structure contents of each sample were calculated using an analysis program SELCON3 and the obtained values are shown in Table 1. Comparing with a previous crystallographic study [1], α-helices and turns were significant in the intrinsically disordered C-tail. The β-strand contents were more explicit for the mutated samples. Interestingly the fraction of the β-strands was noticeably larger in multimers than in dimer.

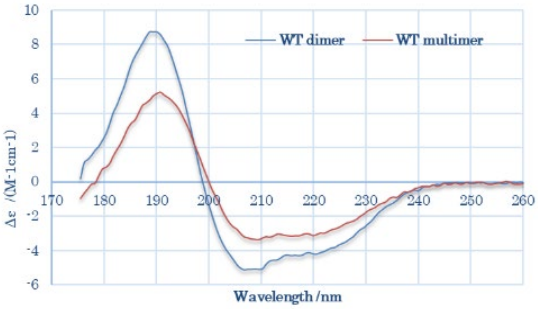

FIGURE 1. CD spectra of the dimer and multimer of wild type XRCC4.

TABLE 1. Secondary structure contents of dimer and multimer of the wild type and mutated XRCC4.

Structure content (%)			α-Helix	β-Strand	Turn	Unordered
Crystallography [1] *			38	26	8	28
CD	Wild type	dimer	50.8±0.9	5.8±0.8	20.1±2.2	23.2±2.1
		multimer	36.4±1.0	15.7±0.8	22.5±1.4	25.4±0.6
	S260D	dimer	50.2±1.9	7.1±3.6	19.7±2.7	23.0±1.2
		multimer	34.2±0.5	17.3±0.9	23.1±0.3	25.5±1.1
	S327D	dimer	47.4±2.1	11.5±4.5	18.4±4.1	22.8±1.3
		multimer	32.0±1.7	19.6±0.8	22.7±0.2	25.7±1.2

* The length of amino-acid sequence is 1th–203rd residues.

SAXS profiles of dimer and multimer of XRCC4

The scattering curve strongly depended on the state of polymerization of XRCC4 (Fig. 2). However, the pseud-phosphorylation did not noticeably affect the scattering pattern. In the low-q region for dimmers, we were able to perform Guinier plot using SAngler 2.1.3 assuming the proteins were a globular shape. For multimer, we found a q-region in which Cross-sectional Guinie plot (inset in the right panel of Fig.2) was applicable by assuming the multimers were rod shape. We obtained radii of inertia (Rg) of the dimers and cross-sectional radii of inertia (Rc) of the multimers. Rg values were about 50Å for the wild type as well as mutated ones. Rc values were slightly larger (roughly 60-70 Å) than Rg for each sample. Thus, the multimers were presumed to be filament like shape.

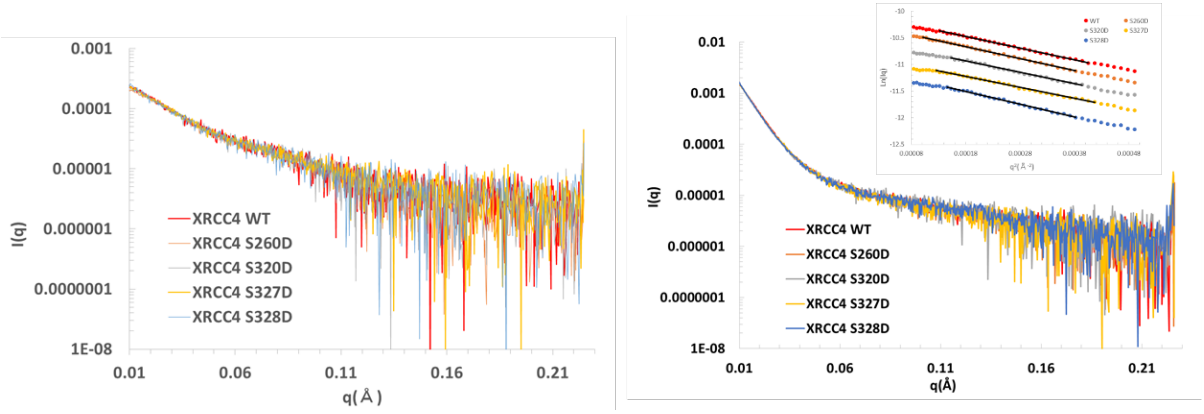

FIGURE 2. SAXS curves of dimers (left) and multimers (right) of wild type and mutated XRCC4. Inset indicates Cross-sectional Guinie plot for the scattering curves of the multimers.

DISCUSSION

The two analyses for the full-length XRCC4 in solution strongly suggest that the intrinsically disordered C-terminal tail plays an important role to induce a conformational change from inactivated homodimer to activated multimer by boosting β-strand formation as indicated by CD measurements. The phosphorylation at the C-terminal may facilitate the multimerization. Multimers formed in this way are filament-like and, presumably, include DNA molecule as a component of the super-molecular-complex of a DSB repair platform (Fig. 3).

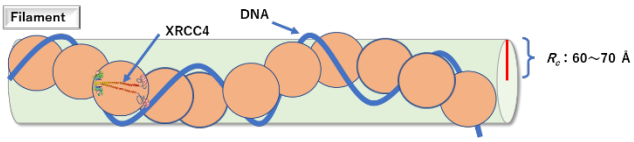

FIGURE 3. A filament model of XRCC4 multimers with DNA.

REFERENCES

1. M. S. Junop, M. Modesti, A. Guarné, R. Ghirlando, M. Gellert, and W. Yang, *EMBO J.* **19**, 5962-59 (2000).